The Intensity of Vibronic Transitions in the Emission Spectrum of the Trivalent Gadolinium Ion

G. BLASSE

Debye Research Institute, University of Utrecht, P.O. Box 80 000, 3508 TA Utrecht (The Netherlands)

and L. H. BRIXNER

E.I. du Pont de Nemours and Company, Central Research and Development Department, Experimental Station, P.O. Box 80356, Wilmington, DE 19880-0356 (U.S.A.)

(Received June 19, 1989)

Abstract

The intensity of the vibronic transitions in the emission spectrum of the Gd^{3+} ion is discussed using new data as well as data from the literature. As model compounds the following compositions are used: (i) the ordered perovskites Ba_2LnTaO_6:Gd (Ln = La, Y, Lu) where Gd^{3+} occupies a site with octahedral symmetry; (ii) the hydroxide $Y(OH)_3$:Gd where purely-cooperative vibronic transitions occur. The vibronic intensities vary by an order of magnitude over the series of compositions under discussion. The relevant theories are summarised. It is shown that they are able to account qualitatively for all trends and phenomena observed.

1. Introduction

In a recent paper we have shown that the emission of the Gd^{3+} ion can be successfully studied by using X-ray excitation [1]. In this way it was possible to observe that the dominating $^6P_{7/2} \rightarrow {}^8S$ electronic emission line is accompanied by vibronic lines, the intensity of which amounts characteristically to 1–10% of that of the electronic line. In this paper we are reporting on the following:

(i) The Gd^{3+} emission of the ordered perovskites Ba_2LnTaO_6:Gd where Gd^{3+} occupies a site with inversion symmetry (Ln = La, Y, Lu).

(ii) The Gd^{3+} emission of $Y(OH)_3$:Gd which is the best example of the simultaneous occurrence of vibronic and cooperative vibronic lines; the spectra have been published recently [2].

(iii) The intensity variation of the Gd^{3+} vibronic lines in a large number of Gd^{3+}-doped host lattices using data published before by ourselves and by others.

The organisation of this paper is as follows. In Section 3 the luminescence of Ba_2LnTaO_6:Gd is discussed, and in Section 4 that of $Y(OH)_3$:Gd. Some related compositions will also be considered. In Section 5 we review briefly the existing theories on the intensity of the vibronic lines of rare-earth ions. In Section 6, finally, we apply the results of the theories to the observations which have been made on the Gd^{3+} vibronic lines.

2. Experimental

The Tantalates

Barium rare-earth tantalates are extremely refractory compositions and need to be prepared at very high temperatures in order to obtain single phase materials. Typically, optical grade Ta_2O_5 (H. Starck Co.), 99.99% pure Ln_2O_3 (Rhone Poulenc) and optical grade $BaCO_3$ (Johnson Matthey, AESAR) are milled together in the appropriate stoichiometry under acetone for about 1 h. After drying, these blends are fired at 1250 °C in air for 8 to 10 h. The reaction product is homogenised via dry milling and pressed into 1 inch diameter pellets, which are fired on recrystallised Al_2O_3 supports at 1600 °C for 4 to 6 h. Materials prepared this way were invariably single phase and were used in this form for the optical measurements.

$Y(OH)_3$

Yttrium hydroxide was prepared hydrothermally; for details on the conditions we refer to ref. 2.

3. The Luminescence of Ba_2LnTaO_6:Gd (Ln = La, Gd, Y, Lu)

The emission spectrum of Ba_2LaTaO_6:Gd under X-ray excitation is shown in Fig. 1. The $^6P \rightarrow {}^8S$ emission around 315 nm is dominating (Fig. 2). There is a weak $^6I \rightarrow {}^8S$ emission around 280 nm and a weak broad band with a maximum at about 330 nm. The total emission intensity is about one order of magnitude lower than for the efficient Gd^{3+} luminescence observed in other host lattices [1]. In Table 1 the

0020-1693/90/$3.50

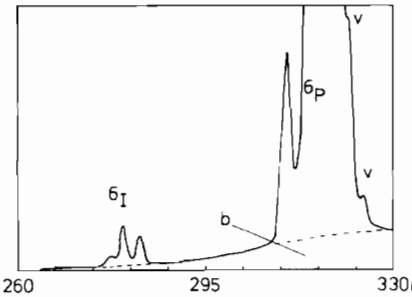

Fig. 1. X-ray excited emission spectrum of Ba_2LaTaO_6:Gd at 300 K. The electronic transitions ^6I, $^6P \rightarrow {}^8S$ are indicated by the initial levels; v indicates vibronic transitions and b the tantalate broad-band emission. The broken line separates the line emission from the band emission.

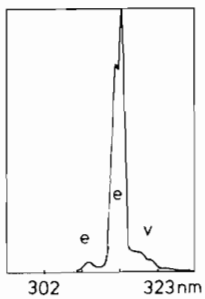

Fig. 2. The $^6P \rightarrow {}^8S$ emission of Fig. 1. The electronic transitions are indicated by e, the vibronic transitions by v.

TABLE 1. Assignment of the emission transitions in X-ray excited Ba_2LaTaO_6:Gd at room temperature

Position (cm^{-1}) of emission features	Assignment	Infrared spectrum (cm^{-1})[c]
36070	$^6I_{11/2} \rightarrow {}^8S$	
35745	$^6I_{9/2,\,17/2} \rightarrow {}^8S$	
35365	$^6I_{7/2} \rightarrow {}^8S$	
32230	$^6P_{5/2} \rightarrow {}^8S$	
31695	$^6P_{7/2} \rightarrow {}^8S$	
31595	$^6P_{7/2} \rightarrow {}^8S$	
31325	e[b] - 320	$\nu_4(TaO_6)$350
31080	e[b] - 565	$\nu_3(TaO_6)$600
30840	e[b] - 805	$\nu_1(TaO_6)$800
30000[a]	TaO_6	

[a]Maximum of broad-band emission. [b]Average of $^6P_{7/2} \rightarrow {}^8S$ components. [c]From Ba_2YNbO_6 [10], see text.

assignment of the total emission spectrum of Ba_2LaTaO_6:Gd is given. The ratio r [1] between the total vibronic intensity and the electronic line intensity amounts to 0.09, a rather high value.

The compositions Ba_2GdTaO_6, Ba_2YTaO_6:Gd and Ba_2LuTaO_6:Gd were also investigated.

Pure Ba_2GdTaO_6 shows only a very weak emission, the spectrum of which is different from the

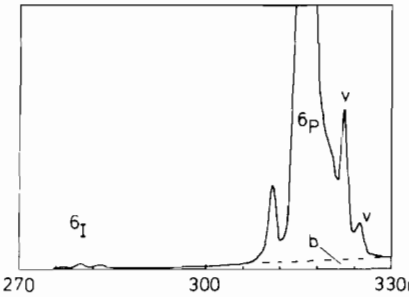

Fig. 3. X-ray excited emission spectrum of Ba_2LuTaO_6:Gd at 300 K. See Fig. 1 for notation.

TABLE 2. Intensity of the vibronic transitions in the emission spectra of the Gd^{3+} ion in Ba_2LnTaO_6 (Ln = La, Y, Lu) at 300 K. The ratio r gives the integrated vibronic intensity relative to the integrated vibronic intensity relative to the integrated electronic intensity of the $^6P_{7/2} \rightarrow {}^8S$ transition

	La	Y	Lu
r (ν_4 vibronic)	~0.04[5]	~0.05	~0.06[5]
r (ν_3 vibronic)	0.03[5]	0.05	0.06[5]
r (ν_1 vibronic)	0.01	0.01	0.01
r (total)	0.09	0.11	0.14

diluted compositions $Ba_2Y_{1-x}Gd_xTaO_6$. We assume that Ba_2GdTaO_6 is concentration quenched and that the emission originates from small amounts of a second phase. In fact the emission spectrum is very similar to that of $YTaO_4$:Gd, pointing to $GdTaO_4$ as the second phase.

The fact that Ba_2GdTaO_6 is quenched is interesting. The shortest Gd–Gd distance (5.7 Å) is so large, that direct Gd–Gd transfer is not expected to have a high probability [3]. This implies that the tantalate group plays an important role as an intermediary in the exchange mechanism as observed also for the Eu^{3+} ion [4, 5].

The luminescence of Ba_2YTaO_6:Gd and Ba_2LuTaO_6:Gd is similar to that of Ba_2LaTaO_6:Gd. However, the intensity of the vibronic lines is different. Figure 3 gives as an example the X-ray excited emission spectrum of Ba_2LuTaO_6:Gd. The higher intensity of the vibronic line which is in the centre of the vibronic part (coupling to ν_3) is immediately clear (compare Figs. 2 and 3). Table 2 gives a survey of these differences. In this Table the r values of the individual vibronic lines are tabulated for the three host lattices. These values are not very accurate; especially the value for the vibronic transition which is close to the electronic transition (coupling to ν_4) is not very reliable for obvious reasons.

As argued elsewhere, we assume that excitation of the Gd^{3+} ions occurs via the TaO_6 octahedra [6, 7]. Since the Gd concentration is 5 at.%,

$0.95^6 = 73\%$ of the tantalate groups have no Gd neighbours. It is known that the tantalate and niobate groups in these ordered perovskites do not luminescence efficiently [8]. This means that a large amount of the tantalate excitation energy is lost non-radiatively. This fact explains why the overall emission intensity is rather low and why the intensity ratio Gd^{3+}/TaO_6 is ~8, whereas it should be 0.37 without non-radiative losses.

Since the tantalate emission maximum overlaps the ^6P levels favourably, the ^6P levels will be populated more effectively than the ^6I levels (see also ref. 7). The $^6I \rightarrow {}^8S$ emission intensity is about 1% of that of the $^6P \rightarrow {}^8S$ emission intensity. Although this seems to confirm the population argument, it implies a peculiar consequence for the $^6I \rightarrow {}^6P$ non-radiative transitions.

The rate of this non-radiative transition can be estimated using the van Dijk–Schuurmans approximation [9]. Using an energy gap of $\Delta E = 2500$ cm^{-1} and the highest vibrational frequency available in the lattice, (~800 cm^{-1}, symmetric tantalate stretching, see below), the non-radiative $^6I \rightarrow {}^6P$ rate amounts to about 3×10^5 s^{-1}. The radiative $^6I \rightarrow {}^8S$ rate will be about 300 s^{-1}, since the Gd^{3+} ion occupies a site with inversion symmetry. This implies that upon ^6I excitation only 1% of the Gd^{3+} emission would originate from the ^6I level. This is in striking contrast with the experimental results which give 1% ^6I emission whereas the ^6P level is populated preferentially. Obviously the tantalate vibrations are not used for the non-radiative transition.

If we use instead of the 800 cm^{-1} frequency of the tantalate group an estimated 250 cm^{-1} frequency for the Gd–(TaO_6) vibration, the non-radiative rate decreases to 3×10^3 s^{-1}.

The spectral overlap of the TaO_6 emission band with the ^6I levels is one order of magnitude less than with the ^6P levels. Our model predicts, therefore, 90% occupation of the ^6P levels and 10% of the ^6I levels. With the 250 cm^{-1} frequency, the $^6I \rightarrow {}^6P$ non-radiative rate is one order of magnitude larger than the $^6I \rightarrow {}^8S$ radiative rate. This accounts very well for the observed 1% ^6I level emission.

Now we turn to the $^6P \rightarrow {}^8S$ emission of the Gd^{3+} ion (Figs. 1–3 and Table 1). The $^6P_{5/2} \rightarrow {}^8S$ emission is thermally activated. The $^6P_{7/2} \rightarrow {}^8S$ (electronic) emission line shows a crystal field splitting for the $^6P_{7/2}$ level of about 100 cm^{-1}. The vibronic lines could easily be assigned using infrared and Raman data of Ba_2YNbO_6 [10]. Here we make use of the fact that the niobate and tantalate vibrational frequencies seldom differ much [11].

Although the vibronic intensities will be discussed below, we draw attention to the fact that the intensity decreases in the sequence Ba_2LuTaO_6:Gd, Ba_2YTaO_6:Gd, Ba_2LaTaO_6:Gd with the exception of the ν_1 vibronic.

4. The Luminescence of $Y(OH)_3$:Gd

The luminescence of $Y(OH)_3$:Gd was reported recently [2]. Here we mention the essential results which are of great importance for this study.

The X-ray excited emission spectrum of $Y(OH)_3$:Gd is very simple. It consists of the $^6P_{5/2}$ and $^6P_{7/2} \rightarrow {}^8S$ emission lines. The latter is accompanied by a relatively strong vibronic line with a maximum at 540 cm^{-1} from the parent electronic line. The ratio r amounts to 8%. This vibronic line can only be due to coupling with the Gd–O vibrations.

Surprisingly enough there is at first sight no vibronic feature due to coupling with the OH^- group. Under high magnification a weak feature could be observed at 353 nm. The ratio r is about 0.2%. It is situated at 3570 cm^{-1} from the electronic origin. Therefore this feature must be due to coupling with the OH^- stretching vibration.

The system $Y(OH)_3$:Gd is very suitable for the study of Gd^{3+} vibronic lines. Only two vibronic lines are observed. The frequencies of the vibrations involved differ an order of magnitude, so that mixing can be neglected. Further the OH^- vibration is not coupled to other hydroxyl groups due to the absence of H-bonding. This means that the OH^- vibration in $Y(OH)_3$ is located in the OH^- group, and that the Gd–(OH) vibration in $Y(OH)_3$:Gd is a vibration of Gd relative to the OH group.

The vibronic line due to OH^- is, therefore, a real cooperative vibronic line [12], whereas the other one is a regular vibronic feature. This will be of importance in the considerations below.

5. Theories on the Intensity of Vibronic Transitions in Rare-earth Spectra

The intensity of vibronic lines in the f–f spectra of rare-earth ions is a complicated problem. Through recent years the following approaches were made.

(a) Faulkner and Richardson [13] gave a general theory of vibronically induced electric-dipole intensity in the f–f transition of octahedrally (O_h) coordinated trivalent rare-earth ions. The model includes static as well as dynamic coupling between the metal ions and the ligands. The calculations relate to elpasolite systems Cs_2NaMCl_6 (M = rare-earth ion(s)). The coupling is with the ν_3, ν_4 and ν_6 vibrational modes of the MCl_6 octahedron. There is good agreement between the experimental results and the calculations.

(b) Judd [14] has put forward a comparable approach for the same system (i.e. MCl_6 octahedron). In the static coupling he considers the interaction between the 4f electrons on M with a spherical charge distribution with net charge –ge (the ligand) and with the dipoles which are induced in the ligands by

the polarising action of the central M^{3+} ion. The induced dipole moment is $3e\alpha\vec{r}_j/r_j^3$, where α is the ligand polarisability, and r_j the distance from the M nucleus to the site j of the displaced ligand.

Further he shows that the dynamic-coupling term runs more or less parallel with the static coupling term. The dynamic term becomes more important if the covalency increases. Under certain conditions both terms are of comparable magnitude. We will present the final result below.

(c) Stavola *et al.* [12] added a new element to the discussion by considering cooperative vibronic transitions, i.e. transitions in which there occurs simultaneously an electronic transition within the 4f shell of M and a vibrational transition within the ligand (for which they took OH^- and H_2O). The emission intensity depends on the infrared oscillator strength of the vibration and R^{-6}, where R is the M–ligand distance.

(d) Dexpert-Ghys and Auzel [15] have compared these approaches and have shown that they overlap. The interaction Hamiltonian in approaches (a) and (b) is the odd vibrating part of the crystal field, and in (c) the Coulombic interaction between the M ion and the vibrating molecular species. It is shown that the static part of (a) and (b) is equivalent to (c). Further these authors state that all approaches neglect the classical one-phonon vibronic replicas (Franck–Condon case). We have shown experimentally that this point has been well taken [16].

At the moment we have available a large amount of data on vibronic intensities of Gd^{3+} in many different host lattices. The theoretical approaches are so complicated that they are not very suitable to analyse our data compilation. Therefore we have taken the general outcome as a basis for the further discussion. In the notation of refs. 14 and 15 it runs as follows

$$P_v \sim \nu(g + n\alpha R^{-3})^2 \Xi(1,2)^2 \langle J \| U^{(2)} \| J' \rangle^2 \times \frac{1}{2J+1} \langle 0 \| T^{(1)} \| p \rangle^2 \quad (1)$$

where P_v is the oscillator strength of the vibronic transition involved, ν its frequency, n the number of ligands around M, g and α the charge and polarisability of the ligand (see above), R the M–ligand distance, $\Xi(1,2)$ is defined by eqn. 14 in ref. 17 and takes care of the opposite-parity mixing, J and J' are the total quantum numbers of the initial and final electronic states, the first matrix element is that of the reduced tensor operator $\|U^{(2)}\|$, and the second matrix element that of the electric dipole operator connecting the initial (0) and final (p) vibrational states.

Considering only vibronics belonging to the $^6P_{7/2} \rightarrow {}^8S$ transition, the J values and the $U^{(2)}$ matrix element will not vary. Note, however, that this matrix element imposes a selection rule on the vibronic transitions, viz. $\Delta J = 0, \pm 2$. The $T^{(1)}$ matrix element predicts the most intense vibronic lines for coupling with the most infrared-intense vibrational transitions.

The term $(g + n\alpha R^{-3})^2$ is hard to analyse. It will vary less with the nature of the ligands than thought of at first sight. A higher value of g implies a lower value of α; an increase of α will usually mean that R increases too. If we consider one and the same ligand, for example oxygen, the value of α might well be different. This will be discussed below.

6. The Intensity of the Vibronic Transitions in the Emission Spectra of Gd^{3+} in Different Host Lattices

To start with we have presented in Table 3 a number of Gd^{3+}-containing compositions for which the value of r is known. This value varies by an order of magnitude. Although this ratio is often used in the literature, it should be realized that its value is not absolute, since the radiative rate of the electronic $^6P_{7/2} \rightarrow {}^8S$ transition varies from compound to compound. For a site with inversion symmetry this transition is purely magnetic-dipole, but if the centre of symmetry is absent it has also electric-dipole character. The radiative vibronic rate can be found by measuring the radiative decay rate of the $^6P_{7/2}$ level, the ratio r and using the calculated radiative rate for magnetic-dipole emission. This has not been

TABLE 3. Ratio r of the total vibronic intensity and the electronic intensity of the $^6P_{7/2} \rightarrow {}^8S$ transition in several host lattices at room temperature

Composition	r	Reference
$Cs_2NaGdCl_6$	0.3	19
La_2O_3:Gd	0.25	21
LaOCl:Gd	0.16	16
Ba_2LnTaO_6:Gd	0.12 (average)	this work
Y_2O_3:Gd	0.12	25
Y_2O_2S	0.11	20
$GdCl_3 \cdot 6H_2O$	0.1	1
$CaWO_4$:Gd	0.09	7
$YTaO_4$:Gd	0.09	7
BaFBr:Gd	0.08	20
Gd acetate$\cdot 4H_2O$	0.08	22
$Y(OH)_3$:Gd [a]	0.08	2, this work
$GdAl_3B_4O_{12}$	0.08	1
CaS:Gd	0.07	23
$ScBO_3$:Gd	0.05	26
$CaCO_3$:Gd	0.03	20, 21
$LaAlO_3$:Gd	0.02	21
[Gd ⊂ 2.2.1]$Cl_3 \cdot 2H_2O$	0.02	24
LaF_3:Gd	0.02	21
$Gd(ClO_4)_3 \cdot 6H_2O$	0.02	27

[a] OH^- contributes only 0.002.

performed for many compositions. Recently such data have been reported for YOCl:Gd [18]. For the compositions in Table 3 we did not perform the decay measurements. This is a formidable job, since the decay time cannot always be interpreted as the radiative rate because of energy migration or energy transfer. The example of $Y(OH)_3$:Gd is illustrative. The Gd^{3+} emission overlaps a weak host lattice absorption band which must reduce the decay rate. Here we will restrict ourselves to a critical survey of the data in Table 3. The table contains especially those cases where r is relatively high; in ref. 1 it has been shown that in many cases r is 0.02–0.03.

First we consider the compositions discussed above. In $Y(OH)_3$:Gd we observed two clearly different types of vibronic transitions. The one due to coupling with the OH^- vibration is of the cooperative type. Stavola *et al.* [12] performed a quantitative calculation of the OH^- vibronic transition belonging to the $^6P_{7/2} \rightarrow {}^8S$ transition, but compared the results to experiments where H_2O is used as a ligand. The infrared oscillator strength of the OH^- ion amounts to $(1–6) \times 10^{-3}$ [28]. With this value they arrived at a radiative rate for coupling with one OH^- group of 0.08 s^{-1} [12]. This yields for nine OH^- groups (as in $Y(OH)_3$:Gd) 0.7 s^{-1}.

For this vibronic transition we find from the spectra $r = 0.002$. If we estimate the total radiative rate to be 300 s^{-1} (a reasonable value for Gd^{3+} on a site without inversion symmetry), the OH^- vibronic rate is about 0.6 s^{-1}. This is a very good agreement with the prediction by Stavola *et al.* [12], where it should be remembered that $Y(OH)_3$:Gd is a perfect system to apply the theory.

For the stretching vibration of H_2O the oscillator strength in the infrared is an order of magnitude larger than for OH^- [15], especially if hydrogen bonding occurs [29]. In fact the r value for H_2O vibronic lines due to coupling of the stretching mode with the $^6P_{7/2} \rightarrow {}^8S$ transition is also an order of magnitude larger than for the OH^- stretching vibration. Examples are $[Gd \subset 2.2.1]Cl_3 \cdot 2H_2O$ (see Table 3), $Gd_2(SO_4)_3 \cdot 8H_2O$ [30], $NaGd(SO_4)_2 \cdot H_2O$ [31], and $Gd(ClO_4)_3 \cdot 6H_2O$ (Table 3).

The coupling with the Gd–$(OH)^-$ vibration in $Y(OH)_3$:Gd is much stronger, yielding $r = 0.08$. This is ascribed to a large value of the product $n\alpha$ in eqn. (1). For $Y(OH)_3$ n amounts 9. The value of α is hard to derive. According to data in ref. 32 it is not much different from that of water, which implies that $\alpha(OH^-)$ is closer to $\alpha(F^-)$ than to $\alpha(O^{2-})$. However, we have to take into account the frequency dependence of α. This can be done by using the formula [33]

$$\alpha(\nu) = \frac{e^2}{m} \sum_j \frac{f_{ij}}{\nu_{ij}^2 - \nu^2} \qquad (2)$$

Here ν is the frequency under consideration, ν_{ij} the absorption frequency and f_{ij} the oscillator strength of the electronic transition between the states i and j. From the diffuse reflection spectrum discussed in ref. 2 it is clear that $\alpha(OH^-)$ at the frequency of the vibronic transition involved will be large, since $\nu_{ij}^2 - \nu^2$ is relatively small. Since $\alpha_o(OH^-)$ is slightly larger than $\alpha_o(F^-)$, viz. 1.75×10^{-24} versus 1.04×10^{-24} cm^3, respectively, and α_ν will be considerably larger for OH^- than for F^- because the optical absorption transition is at lower energy for the hydroxide than for the fluoride, it becomes clear that the vibronic transitions in Gd^{3+}-doped fluorides will be considerably less intense (see LaF_3:Gd in Table 3).

Let us now consider Ba_2LaTaO_6:Gd. In this host lattice the Gd^{3+} ion has site symmetry O_h and is coordinated by six tantalate octahedra which have also O_h site symmetry. The emission spectrum of the Gd^{3+} ion shows three vibronics due to coupling with the ν_3, ν_4 and ν_1 modes of the tantalate group (see Figs. 1 and 2 and Table 1). The ν_3 and ν_4 modes appear as strong bands in the infrared spectrum [10], so that their occurrence in the vibronic spectrum is not unexpected. However, the symmetric stretching mode ν_1 does not appear in the infrared spectrum. The matrix element $\langle 0 \| T^{(1)} \| p \rangle$ is zero for this vibration, so that eqn. (1) gives also zero for the vibronic transition involving ν_1. Nevertheless it is observed with an r ratio of about 0.01.

This vibronic transition is ascribed to a Franck–Condon vibronic replica. The coupling parameter S can be estimated from the r value using the expression $e^{-s} = I(\text{o-o})$, where $I(\text{o-o})$ gives the relative intensity of the zero-phonon (or pure electronic) transition [34]. From $e^{-s} = 0.99$ we find $S = 0.01$. Such a low value is not unexpected for the rare-earths ions and was also used in ref. 15. A vibronic line due to coupling with a totally symmetric vibrational mode with comparable relative intensity has been observed before in many other compositions: for example $Cs_2NaGdCl_6$ [19], $YTaO_4$:Gd [7], $GdAl_3B_4O_{12}$ [1], $BaSO_4$:Gd [1] and $BaCO_3$:Gd [1].

The vibronic transitions involving ν_3 and ν_4 are more intense. These modes are infrared active. In the infrared spectrum these modes have about equal intensity, as in the vibronic spectrum. The relatively high intensity of the ν_3 and ν_4 vibronic transitions is ascribed to a relatively high value of α. It should be realized that the tantalate group in Ba_2GdTaO_6 shows a broad absorption band with a maximum at 41 700 cm^{-1} [35]. For Ba_2LaTaO_6 this result will not be much different. Equation (2) then predicts an increase of α, especially so, since the value of f_{ij} is also high for the tantalate absorption transition.

In $YTaO_4$:Gd the situation is comparable. Here $n = 8$ (instead of 6), α is somewhat lower due to the fact that the absorption edge is at 44 500 cm^{-1} [36], but R is somewhat smaller the M–O–Ta angle being

less than 180° (the value in the ordered perovskite). The intensity of the vibronic lines is only slightly less than in the perovskite (see Table 3).

Table 2 shows that the r values for Gd^{3+} in the ordered perovskites Ba_2LnTaO_6 (Ln = La, Y, Lu) depend on Ln. Note that this is not the case for the phonon replica due to coupling with ν_1. The intensity of the vibronic transitions due to coupling with ν_3 and ν_4 should obey eqn. (1). However, this equation does not contain a term which is expected to vary from La to Lu. Since the space available for the Gd^{3+} ion decreases from La to Lu, the covalency will increase. According to Judd [14] and Faulkner and Richardson [13] increasing covalency results in higher vibronic intensity. We assume that the series Ba_2LnTaO_6:Gd, where the properties involved do not vary with the choice of Ln, is a fine example of the prediction that the vibronic intensity increases with increasing covalency.

In the elpasolite (i.e. ordered perovskite) $Cs_2NaGdCl_6$ r amounts to 0.3. There are no molecular vibrational modes. Coupling occurs with the modes of the regular $GdCl_6^{3-}$ octahedron [19]. The values of α for Cl^- and O^{2-} are practically equal [33]. It is questionable, however, whether these ionic α values are useful in this connection. The Cl^- ion in elpasolite is strongly polarised towards the Gd^{3+} ion, the ion on the other side of the anion being Na^+. This is a favourable situation for high vibronic intensity, as we will see below. Also, this configuration will result in a higher degree of covalency which promotes also higher intensity (see above). Finally, R will be shorter than for the tantalate perovskite.

Now we consider the other compositions in Table 3 which lack molecular (internal) vibrations. They are all characterised by a high value of r, except LaF_3:Gd. Fluorides are expected to give low vibronic intensities in view of the low value of α and the low degree of covalency. The compositions La_2O_3:Gd and Y_2O_3:Gd show high values of r, where the former gives more intense vibronics than the latter. These compounds are rather covalent, and α will be increased by the presence of a low-lying host lattice absorption (La_2O_3 44 000 cm^{-1}, Y_2O_3 47 500 cm^{-1} [37]).

The r value for CaS:Gd (0.07) is not as high as expected at first sight in view of the high value of α (S^{2-}), viz. 10.2×10^{-24} cm^3 [33], and the low optical absorption edge (33 600 cm^{-1}, [23]). However, the high value of α is counteracted by the increase of R. More important seems the symmetric coordination of the S^{2-} ions in the rocksalt structure of CaS. This reduces the possibility to polarise the S^{2-} ion towards the Gd^{3+} ion which will occur only due to the presence of an effective positive charge on the Gd^{3+} ion. In the compound with layered structure LaOCl:Gd, α is expected to be larger, and r is much higher. In BaFBr:Gd, isomorphous with LaOCl:Gd, the value of r decreases again: the fluoride ion will not contribute strongly, and the bromine ion has a very large radius. In this connection it is also interesting to note that it has been shown that the polarisability of oxygen in an anisotropic surroundings increases with the twelfth power of the anion–cation distance [38]. The other compound with layered structure, viz. Y_2O_2S:Gd, has a relatively low r value. In this structure the S^{2-} ions are octahedrally coordinated by the rare earth ions, and the O^{2-} ions tetrahedrally. As in the rocksalt structure, this is not so favourable for polarisation.

In most of the oxidic coordinations with absorption transitions in the vacuum UV the value of r does not exceed a few percent. $ScBO_3$:Gd, and especially $GdAl_3B_4O_{12}$, seem to have rather high r values (see Table 3). Perhaps the small distance R, due to the six-coordination of Gd^{3+} and the bent Gd–O–B angle, play a role here. The former favours covalency, the latter a shorter distance.

The high r value for the Gd acetate is related to the low absorption transition of the acetate group which roughly coincides with the $^8S \rightarrow {}^6P$ transition on the Gd^{3+} ion [21].

A very exceptional case seems to be MgF_2:Gd^{3+} reported by ourselves with an r value of about 1 [39]. As far as the assignments of the lines is concerned, there is no reason to become suspicious. However, the present results show clearly that an r value of 1 is unrealistic, and that the assignment, how obvious it may have been, is incorrect. Accepting the fact that the vibronic transitions in a fluoride cannot have a higher intensity than a few percent of the electronic origin, we arrive at the following correction of our previous interpretation. The strong lines ascribed to one-phonon vibronics in ref. 39 are interpreted as electronic transitions on the Gd–O associate, already proposed in ref. 39. Unfortunately they are situated at a distance from the electronic lines of the unassociated Gd^{3+} ion which equals the vibrational frequencies of MgF_2. In this way the vibronic transitions belonging to the unassociated Gd^{3+} ion are completely overlapped by the electronic transitions of the associated Gd^{3+} ion.

7. Conclusions

Vibronic intensities in rare-earth spectra have until now been approached either theoretically or experimentally on one given host lattice. Here we have given an overview of the vibronic transitions belonging to the $^6P_{7/2} \rightarrow {}^8S$ emission transition of the Gd^{3+} ion. The vibronic intensities vary by one order of magnitude. By using the general theoretical expression for this intensity, it was possible to account for the large variations observed.

References

1 G. Blasse and L. H. Brixner, *Eur. J. Solid State Inorg. Chem.*, in press, and refs. therein.
2 G. Blasse, L. H. Brixner and S. Mroczkowski, *J. Solid State Chem., 82* (1989) 303.
3 G. Blasse, H. S. Kiliaan and A. J. de Vries, *J. Luminescence, 40/41* (1988) 639.
4 G. Blasse, *J. Chem. Phys., 46* (1967) 2583; J. P. M. van Vliet, D. van der Voort and G. Blasse, *J. Luminescence, 42* (1989) 305.
5 M. Buijs, G. Blasse and L. H. Brixner, *Phys. Rev. B, 34* (1986) 8815.
6 M. K. Crawford, L. H. Brixner and G. Blasse, *Fall Meet. Electrochem. Soc., Chicago, Oct. 1988,* Abstr. 638; to be published.
7 G. Blasse and L. H. Brixner, *J. Solid State Chem., 82* (1989) 151.
8 G. Blasse, *Inorg. Chim. Acta, 157* (1989) 141.
9 J. M. F. van Dijk and M. F. H. Schuurman, *J. Chem. Phys., 78* (1983) 5317.
10 G. Blasse and A. F. Corsmit, *J. Solid State Chem., 6* (1973) 513.
11 G. Blasse, *J. Solid State Chem., 7* (1973) 169.
12 M. Stavola, L. Isganitis and M. G. Sceats, *J. Chem. Phys., 74* (1981) 4228.
13 T. R. Faulkner and F. S. Richardson, *Mol. Phys., 35* (1978) 1141.
14 B. R. Judd, *Phys. Scr., 21* (1980) 543.
15 J. Dexpert-Ghys and F. Auzel, *J. Chem. Phys., 80* (1984) 4003.
16 G. Blasse, J. Sytsma and L. H. Brixner, *Chem. Phys., Lett., 155* (1989) 64.
17 B. R. Judd, *Phys. Rev., 127* (1962) 750.
18 J. Sytsma, G. Blasse and G. F. Imbusch, *J. Chem. Phys., 91* (1989), in press.
19 A. J. de Vries and G. Blasse, *J. Chem. Phys., 88* (1988) 7312.
20 L. H. Brixner, unpublished measurements.
21 W. van Schaik, J. Sytsma and G. Blasse, unpublished measurements.
22 G. Blasse and L. H. Brixner, *Recl. Trav. Chim. Pays-Bas,* in press.
23 W. Lehmann, *J. Luminescence, 5* (1972) 87.
24 G. Blasse, L. H. Brixner and N. Sabbatini, *Chem. Phys. Lett., 158* (1989) 504.
25 L. H. Brixner and G. Blasse, *J. Electrochem. Soc.,* in press.
26 G. Blasse and G. J. Dirksen, *Inorg. Chim. Acta, 145* (1988) 303.
27 G. Blasse and L. H. Brixner, *Inorg. Chim. Acta, 161* (1989) 13.
28 B. Wedding and M. V. Klein, *Phys. Rev., 177* (1969) 1274.
29 H. Siebert, *Anwendungen der Schwingungsspektroskopie in der Anorganischen Chemie,* Springer, Berlin, 1966.
30 M. K. Crawford, L. H. Brixner and G. Blasse, *J. Solid State Chem.*, in press.
31 G. Blasse, *Inorg. Chim. Acta, 132* (1987) 273.
32 E. A. Moelwyn-Hughes, *Physical Chemistry,* Pergamon, Oxford, 1961.
33 C. Kittel, *Introduction to Solid State Physics,* Wiley, New York, 5th edn., 1976.
34 G. F. Imbusch, in M. D. Lumb (ed.), *Luminescence Spectroscopy,* Academic Press, London, 1978, Ch. 1.
35 G. Blasse and A. Bril, *Z. Phys. Chem. N.F., 57* (1968) 187.
36 G. Blasse and A. Bril, *J. Luminescence, 3* (1970) 109.
37 R. C. Ropp, *J. Electrochem. Soc., 111* (1964) 311.
38 H. Bilz, H. Büttner, A. Bussmann-Holder and P. Vogl, *Ferroelectrics, 73* (1987) 493.
39 G. Blasse and L. H. Brixner, *Mater. Res. Bull., 24* (1989) 363.